An experimental and computational study of the unimolecular-decay reaction of diethyl-substituted Criegee Intermediate $(C_2H_5)_2COO$

Jari Peltola[a,*], Timo T. Pekkanen[a,b,*], Petri Heinonen[a], Pyry Salomaa[a], Nino Runeberg[a,c], György Lendvay[b], Arkke J. Eskola[a,**]

[a] *Department of Chemistry, University of Helsinki, P.O. Box 55 (A.I. Virtasen aukio 1), 00014 Helsinki, Finland*
[b] *Institute of Materials and Environmental Chemistry, Research Centre for Natural Sciences, Magyar Tudósok krt. 2., Budapest H-1117, Hungary*
[c] *CSC – IT Center for Science, P.O. Box 405, FI-02101 Espoo, Finland*

Supplemental Material

---

*These authors contributed equally to this work.
**Corresponding author:
Email address: arkke.eskola@helsinki.fi (Arkke J. Eskola)

1. Experiments

A schematic figure of the time-resolved, broadband, cavity-enhanced absorption spectroscopy (TR-BB-CEAS) apparatus utilising UV absorption to detect pentan-3-oneoxide ($(C_2H_5)_2COO$) is shown in Figure S1 and has been described in detail in our previous publications [1, 2]. From here on, we refer to $(C_2H_5)_2COO$ with the acronym DECI (diethyl-substituted Criegee intermediate). Figure S2a shows the cavity transmission as a function of wavelength, whilst Fig. S2b shows the effective optical path length (OPL) of the TR-BB-CEAS cavity as a function of wavelength (300–450 nm). The OPL was determined from

$$A_\lambda(NO_2) = \ln\left(\frac{I_{0,\lambda}}{I_\lambda}\right) = \sigma_\lambda(NO_2) \times [NO_2] \times OPL_\lambda$$
$$OPL_\lambda = \frac{A_\lambda(NO_2)}{\sigma_\lambda(NO_2) \times [NO_2]} \,. \tag{S1}$$

Here $I_{0,\lambda}$ is the light intensity at wavelength λ in the absence of NO_2, I_λ is the light intensity at wavelength λ in the presence of NO_2, $\sigma_\lambda(NO_2)$ is the NO_2 absorption cross section at wavelength λ, $[NO_2]$ is the NO_2 concentration, and the OPL_λ is the effective optical path length at wavelength λ. The OPL was determined at 296 K in a (5.07±0.10) ppm sample of NO_2 in 20 Torr of N_2. The average effective OPL_λ at 340 nm (with the wavelength resolution of 4 nm) is about 75 m. The initial concentration of DECI is estimated from the measured initial absorbance, $A^{DECI}_{0,340\,nm}$, at 340 nm as

$$[DECI]_0 = \frac{A^{DECI}_{0,340\,nm}}{\sigma^{DECI}_{340\,nm} \times OPL} \,. \tag{S2}$$

Note that the absorption cross section $\sigma^{DECI}_{340\,nm}$ (or that of $(C_2H_5)_2CIBr$) has

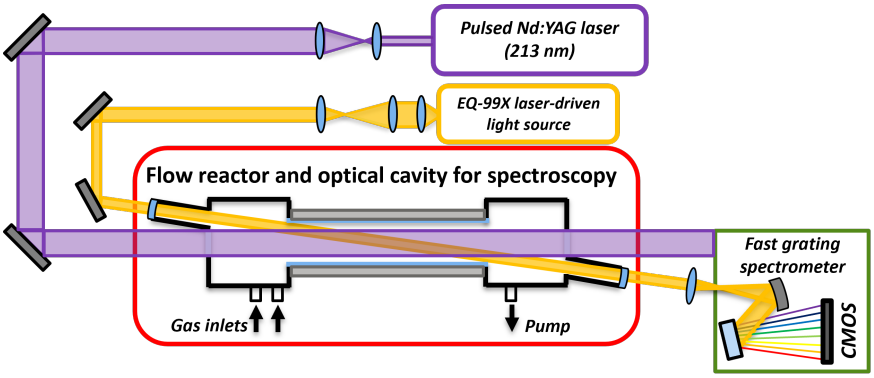

Figure S1: A schematic figure of the time-resolved, broadband, cavity-enhanced absorption spectrometer. DECI is produced from the $(C_2H_5)_2CIBr$ photolytic precursor along a flow tube reactor by a single-pass photolysis laser pulse at 213 nm. DECI is detected by overlapping incoherent laser-driven broadband light source. The sensitivity of the detection is enhanced using an optical cavity formed by two highly reflecting concave mirrors between 300 and 450 nm. The time-dependent broadband absorption spectrum of DECI is measured by a grating spectrometer combined with a fast CMOS line array camera.

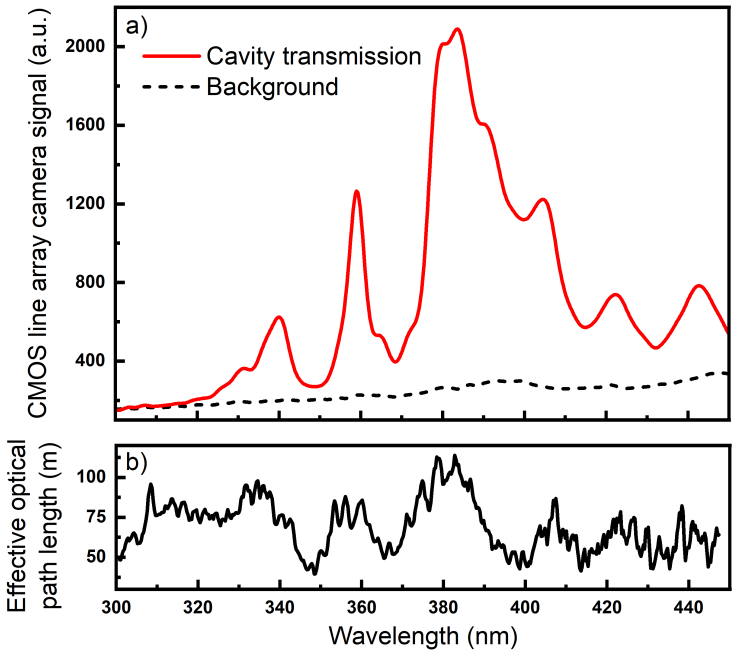

Figure S2: a) The cavity transmission signal. b) The effective optical path length of the TR-BB-CEAS apparatus as a function of wavelength.

not been measured and is unknown at 340 nm. To estimate $[\mathrm{DECI}]_0$, we assume that $\sigma^{\mathrm{DECI}}_{340\,\mathrm{nm}}$ is of the same order of magnitude as those of propan-2-oneoxide (DMCI, $(CH_3)_2COO$) [3] and propanaloxide ($(C_2H_5)C(OO)H$) [4], which are both about 2×10^{-17} cm^2 molecule^{-1} at 340 nm. Of all measurements, the highest peak absorbance signal of about 0.024 gives the highest initial concentration of about 1.6×10^{11} cm^{-3} for DECI. Thus, $[\mathrm{DECI}]_0$ was estimated to be $\leq 2 \times 10^{11}$ cm^{-3}.

The external cooling bath circulation (Huber CC-905) based cooling method of the flow tube reactor is described in our previous publications [2, 5]. All the gases were pre-cooled close to the setpoint temperature before entering the reactor. In the temperature range considered in this study (223–296 K), the temperature variation along the reactor did not exceed ±1.5 K.

2. Synthesis of the precursor

3-Bromopent-2-ene was prepared by the modification of the published procedure [6]. A solution of triphenylphosphite (81.2 g, 0.262 mol) in dry dichloromethane was cooled to -60 °C and bromine (45,6 g, 0.286 mol) was added slowly over 2 h. The mixture was stirred an additional 30 min and pentan-3-one (20.5 g, 0.238 mol) and dry triethyl amine (43.1 ml, 0.309 mol) were added. The reaction mixture was allowed to warm slowly to room temperature and stirred for 18 h at room temperature, and then refluxed for an additional 3 h. Most of the solvent was removed by distillation under normal pressure. The residue was diluted with pentane and the mixture filtered through a short pad of silica.

The solvents were removed by distillation in normal pressure and the product distilled at 110–112 °C. The title compound was obtained as a 1:5 mixture of (*E*)- and (*Z*)-isomers (17.9 g, 51%). The spectroscopic analysis corresponded to the published data [7]. (*E*)-isomer: ^{1}H NMR (400 MHz, $CDCl_3$) δ 5.88 (1H, q, J = 7.1 Hz), 2.47 (3H, m), 1.65 (3H, d, J = 7.1 Hz), 1.12 (3H, t, J = 7.4 Hz). (*Z*)-isomer: 1H NMR (400 MHz, $CDCl_3J$) δ 5.72 (1H, m), 2.47 (3H, m), 1.74 (3H, m), 1.34 (3H, t, J = 7.4 Hz).

In the synthesis of 3-bromo-3-iodopentane, 3-bromopent-2-ene (31.2 g, 0.21 mol) was dissolved in trifluoroacetic acid (60 ml) and concentrated aqueous hydroiodic acid (57 wt%, 31.5 ml, 0.24 mol) was added. The reaction was monitored by ^{1}H NMR and stopped after 75 min. The reaction mixture was diluted with pentane, washed 3 times with water, then with 10% aq $Na_2S_2O_3$ and finally with water 3 more times. The organic phase was dried over $MgSO_4$ and evaporated. Distillation at reduced pressure (70 °C, 8 Torr) gave the title compound (14.3 g, 25 %). ^{1}H NMR (400 MHz, $CDCl_3$) δ 2.45 – 2.38 (2H, m), 2.30 – 2.23 (2H, m), 1.21 (6H, t, J = 7.1 Hz). ^{13}C NMR (100 MHz, $CDCl_3$) δ 55.9, 46.4, 14.4.

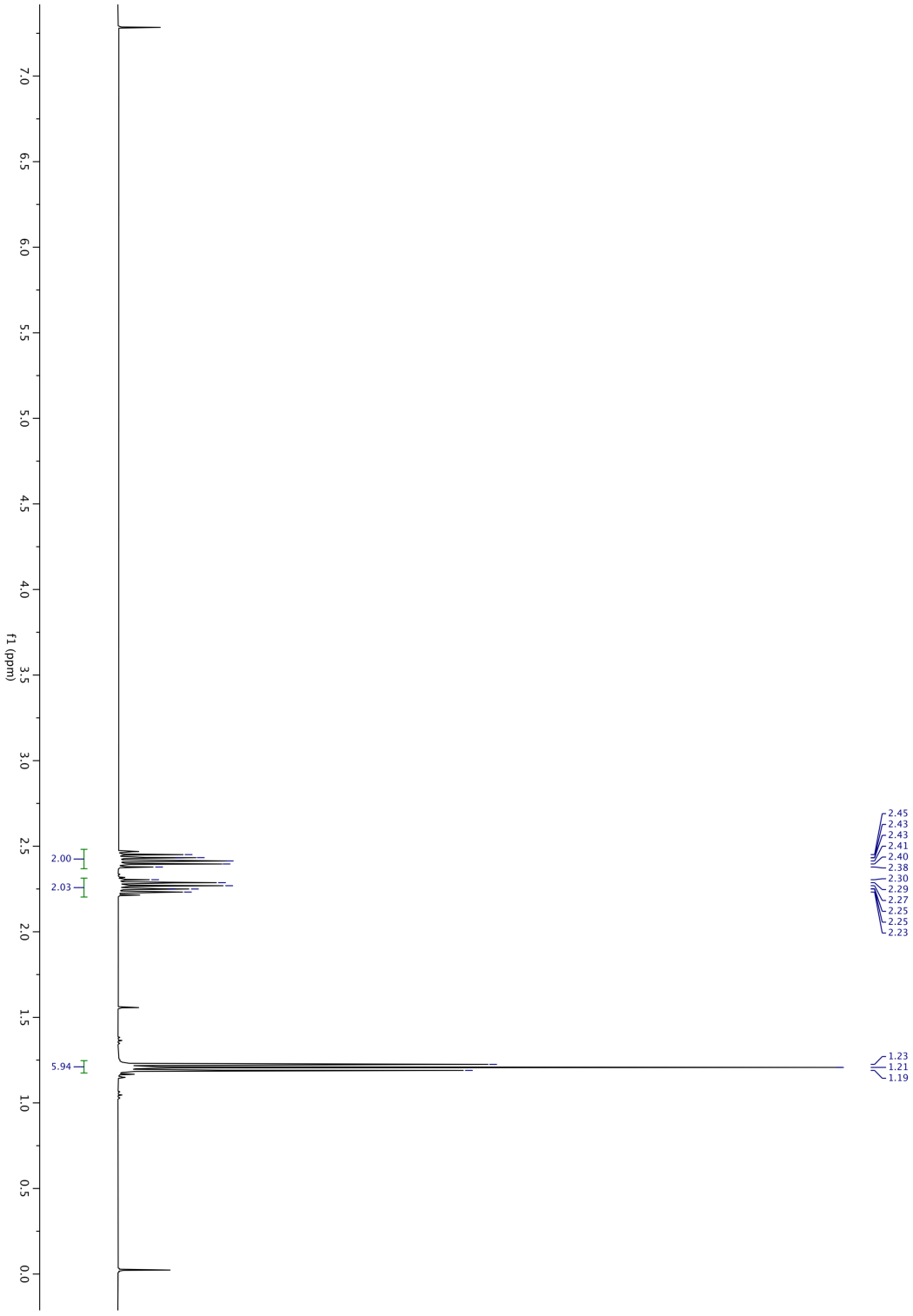

Figure S3: 400 MHz ^{1}H NMR spectrum of 3-bromo-3-iodopentane in $CDCl_3$.

3. Unimolecular-decay reaction of DECI

As is mentioned in the main text, the observed decay of DECI mainly contains contributions from its unimolecular-decay reaction and self-reaction, but also contains small contributions from its diffusion out of the observation region and possible reactions with other reactive species. The rate law to describe the overall loss of DECI can be written as

$$\begin{aligned} -\frac{\mathrm{d[DECI]}}{\mathrm{d}t} &= k_{\mathrm{uni}}[\mathrm{DECI}] + 2k_{\mathrm{self}}[\mathrm{DECI}]^2 + k_{\mathrm{loss}}[\mathrm{DECI}] + k_{\mathrm{bi}}[\mathrm{X}][\mathrm{DECI}] \\ &= (k_{\mathrm{uni}} + k_{\mathrm{loss}} + 2k_{\mathrm{self}}[\mathrm{DECI}] + k_{\mathrm{bi}}[\mathrm{X}])[\mathrm{DECI}], \end{aligned} \tag{S3}$$

where k_{uni} is the unimolecular-decay rate coefficient, k_{self} is the self-reaction rate coefficient, [X] is the total concentration of other possible reactive species contributing to the bimolecular loss (originating, for example, from DECI + $\mathrm{Br}^{\bullet}$ and DECI + $(\mathrm{C_2H_5})_2\mathrm{CI(OO)}$ reactions) with a combined rate coefficient k_{bi}, and k_{loss} is the diffusive-loss rate coefficient. Although the self-reaction rate coefficient k_{self} is probably large, on the order of 10^{-10} $\mathrm{cm^3\ s^{-1}}$, the main contribution to the overall loss rate of DECI comes from the unimolecular-decay reaction due to the low initial DECI concentrations employed in the experiments ($[\mathrm{DECI}]_0 \leq 2 \times 10^{11}$ $\mathrm{cm^{-3}}$).

In analysing the kinetic traces, we used a simplified model

$$\begin{aligned} -\frac{\mathrm{d[DECI]}}{\mathrm{d}t} &= (k_{\mathrm{uni}} + k_{\mathrm{loss}} + k_{\mathrm{eff}}[X_{\mathrm{eff}}])[\mathrm{DECI}] \\ &= k_{\mathrm{DECI}}[\mathrm{DECI}]. \end{aligned} \tag{S4}$$

in which the term $2k_{\mathrm{self}}[\mathrm{DECI}] + k_{\mathrm{bi}}[\mathrm{X}] \approx k_{\mathrm{eff}}[X_{\mathrm{eff}}]$ is approximated to remain constant. Integrating the above rate law gives

$$[\mathrm{DECI}](t) = [\mathrm{DECI}]_0 \mathrm{e}^{-k_{\mathrm{DECI}}t}\ . \tag{S5}$$

This simplified approach to describe the loss of DECI and the use of a single-exponential fitting method has been tested previously by Smith et al. [8] and us [2] in a similar study to determine the unimolecular-decay rate coefficient of $(\mathrm{CH_3})_2\mathrm{COO}$ (DMCI). The single-exponential function fits reasonably well to the kinetic traces, although the observed absorbance can be slightly higher than the fitted value just after the photolysis. In the main text, Figure 5c shows the linear relationship between the obtained k_{DECI} values and $[\mathrm{DECI}]_0$ at 296 K and 10 Torr and 233 K and 7.8 Torr. The linear behaviour suggests that $[X_{\mathrm{eff}}]$ is proportional to $[\mathrm{DECI}]_0$. This is expected since most of the reactive species, as well as DECI, are formed at small concentrations proportional to $[(\mathrm{C_2H_5})_2\mathrm{CIBr}]_0$ and the laser pulse energy (assuming there are no other reactive species in the precursor mixture). At the limit $[\mathrm{DECI}]_0 \to 0$ all secondary chemistry is suppressed (i.e. $(\mathrm{C_2H_5})_2\mathrm{COO} + \mathrm{Br}^{\bullet}$ and $(\mathrm{C_2H_5})_2\mathrm{COO}$ + $(\mathrm{C_2H_5})_2\mathrm{C(OO)I}$ reactions), and so $k_{\mathrm{uni}} + k_{\mathrm{loss}}$ can be obtained from the intercept of a straight line fitted to k_{DECI} versus $[\mathrm{DECI}]_0$ data. Although a more accurate kinetic models would give better fits to the absorption traces, the intercept values of the more accurate and simplified models would be almost the same since the reactive species are formed at small concentrations (see Smith et al. [8]).

As it was also mentioned in the main text, the entire experimental trace signal has two distinct components: a fast-decay and a slow-decay component. The former originates from the absorption of DECI, while the latter corresponds to an absorbance caused by nonreactive specie(s) formed by photolysis, the DECI + O_2 reaction, and/or the unimolecular-decay reaction of DECI. Thus, to fit the measured kinetic traces, we used the functional form

$$A(t) = A_0^{\mathrm{DECI}} \mathrm{e}^{-k_{\mathrm{DECI}} t} + \frac{A_{\mathrm{NR}} k_{\mathrm{DECI}}}{k_{\mathrm{NR}} - k_{\mathrm{DECI}}} \left(\mathrm{e}^{-k_{\mathrm{DECI}} t} - \mathrm{e}^{-k_{\mathrm{NR}} t} \right) + A_{\mathrm{OS}} \ , \qquad \text{(S6)}$$

where $A(t)$ is the measured absorbance at time t, A_0^{DECI} is the absorbance of DECI at $t = 0$, k_{DECI} and k_{NR} are the overall loss rate coefficients for DECI and non-reactive species, respectively, A_{NR} is a fitting parameter, and A_{OS} is a possible measurement offset caused by the TR-BB-CEAS apparatus. In fitting the kinetic trace with the above equation, we assume that the nonreactive species are formed at the same rate as DECI decays and absorb at the detection wavelength. The slow-decay component was observed in all kinetic measurements, but especially in the measurements using higher $[\mathrm{DECI}]_0$ and higher total pressure (see Fig. 5a and 5b). Under constant temperature and pressure, the absorption of nonreactive specie(s) was observed to increase with $[(C_2H_5)_2COO]_0$, but maintained its relative value with respect to DECI absorbance. However, the value of additional absorption relative to DECI absorbance increases with pressure, which may originate from an enhanced stabilization of the $(C_2H_5)_2C(OO)I$ radical. As the yield of $(C_2H_5)_2CI(OO)$ increases with pressure, there will be a corresponding decrease in the yield of DECI.

Another complication in Criegee-intermediate measurements is that the photolytic precursors can absorb in the 340 nm region. This can cause a negative baseline shift in the absorption signal since the precursor concentration drops after photolysis. However, we have found that the baseline shift is negligible for bromo-iodo precursors, which absorb much weaker at 340 nm than di-iodo precursors.

The diffusive-loss rate coefficient (k_{loss}) of DECI was determined using the diffusive-loss rate coefficient of CH_2OO measured by the TR-BB-CEAS-apparatus under the same experimental conditions as in this work [2, 9]. The unimolecular-decay rate coefficient of CH_2OO is negligible below 375 K. In this work, we approximate the diffusive-loss rate coefficient for DECI from

$$k_{\mathrm{loss}}^{\mathrm{DECI}} = \frac{D^{\mathrm{C_5H_{10}O_2}}}{D^{\mathrm{HCOOH}}} k_{\mathrm{loss}}^{\mathrm{CH_2OO}} = 0.43 k_{\mathrm{loss}}^{\mathrm{CH_2OO}} \ , \qquad \text{(S7)}$$

where $D^{\mathrm{C_5H_{10}O_2}}$ and D^{HCOOH} are the diffusion coefficients of methanoic acid and 3-methylbutanoic acid, respectively. Table S1 tabulates the $k_{\mathrm{loss}}^{\mathrm{DECI}}$ values employed in the present work.

Table S1: The $k_{\text{loss}}^{\text{DECI}}$ determined from the previously measured $k_{\text{loss}}^{\text{CH}_2\text{OO}}$ values under the same experimental conditions as used in this work. The $k_{\text{loss}}((\text{C}_2\text{H}_5)_2\text{COO})$ values are calculated as $0.43 \times k_{\text{loss}}(\text{CH}_2\text{OO})$.

T(K)	$[\text{N}_2]$ ($\times 10^{17}$ cm^{-3})	[a] $k_{\text{loss}}^{\text{CH}_2\text{OO}}$ (s^{-1})	$k_{\text{loss}}^{\text{DECI}}$ (s^{-1})
$223 - 296$	1.6	30	13
	3.3	20	9
	16	10	4
	33	7	3

[a] The $k_{\text{loss}}(\text{CH}_2\text{OO})$ values at 223-233 K and 243–296 K were measured in our previous studies [9] and [2], respectively.

Table S2: The experimental conditions and results of the unimolecular-decay-rate-coefficient measurements for the $(CH_3)_2COO \xrightarrow{k_{uni}}$ Products reaction (**DMCI**). These results are from our previous publication [2] and retabulated for ease of comparison (see Table S2).

T (K)	[M] ($\times 10^{17}$ cm^{-3})	p^a (Torr)	k_{DMCI} (s^{-1})	k_{loss} (s^{-1})	$k_{uni}^{(exp)}$ (s^{-1})	$k_{uni}^{(ME)}$ (s^{-1})
296[b]	1.6	5.00	566 ± 24	52	514	502
	3.3	10.0	608 ± 28	32	576	566
	16	500	733 ± 14	15	718	702
	33	100	826 ± 22	12	814	751
	65	200	870 ± 22	10	860	792
310[b]	1.6	5.20	884 ± 34	52	832	818
	3.3	10.5	951 ± 60	32	919	952
	16	52.3	1350 ± 30	15	1340	1250
	33	105	1420 ± 50	12	1400	1370
	65	210	1580 ± 160	10	1570	1480
323[b]	1.6	5.50	1170 ± 180	52	1120	1260
	3.3	10.9	1590 ± 150	32	1560	1500
	16	54.5	2350 ± 50	15	2330	2100
	33	109	2490 ± 40	12	2480	2350
	65	218	2930 ± 90	10	2920	2580
330[b]	1.6	5.60	1570 ± 20	52	1510	1570
	3.3	11.2	2070 ± 120	32	2030	1890
	16	55.7	3340 ± 80	15	3330	2730
	33	112	3330 ± 150	12	3320	3100
340[b]	1.6	5.80	1660 ± 100	52	1610	2120
	3.3	11.7	3000 ± 30	32	2970	2620
	16	57.5	4420 ± 420	15	4410	3940
243[c]	1.6	4.10	91.0 ± 12.0	16	75.0	63.1
	3.3	8.20	87.0 ± 8.0	10	77.0	64.5
	16	41.0	68.0 ± 14.0	5	63.0	66.3
	33	82.0	51.0 ± 16.0	4	47.0	67.0
253[c]	1.6	4.30	118 ± 10	16	102	97.6
	3.3	8.50	115 ± 10	10	105	101
	16	42.6	118 ± 6	5	113	106
	33	85.3	110 ± 26	4	106	107
263[c]	1.6	4.40	163 ± 8	16	147	150
	3.3	8.90	170 ± 16	10	160	157
	16	44.3	153 ± 20	5	148	168
	33	88.7	147 ± 18	4	143	171
273[c]	1.6	4.60	239 ± 12	16	223	228
	3.3	9.20	264 ± 46	10	254	243
	16	46.0	262 ± 24	5	257	267
	33	92.1	279 ± 6	4	275	274
283[c]	1.6	4.80	337 ± 56	16	321	344
	3.3	9.60	321 ± 40	10	311	371
	16	47.9	449 ± 20	5	444	422
	33	95.5	417 ± 48	4	413	437
296[c]	1.6	5.00	605 ± 36	16	589	573
	3.3	10.0	627 ± 62	10	617	634
	16	50.0	856 ± 46	5	851	755
	65	200	902 ± 42	4	899	828
310[c]	3.3	10.5	1090 ± 120	10	1080	1100
	16	52.3	1360 ± 230	5	1350	1380

[a] The fixed $[O_2]$ was $\sim 4 \times 10^{16}$ cm^{-3}. [b] bath gas: He. [c] bath gas: N_2.

4. Computational Results

Table S3: Zero-kelvin relative enthalpies for stationary points on the DMCI (propan-2-oneoxide) potential-energy surface. The energies are in kJ mol^{-1}. Symmetry numbers for the species are also specified. The fitting errors are 1σ. The **bolded** numbers are the values used in the master-equation simulations.

Species	$\sigma_{ext} \cdot \sigma_{int}/m_{opt}$ [a]	W2X // CASPT2(8,7) / aug-cc-pVTZ	W2X // MN15 / Def2TZVP	W3X-L // CASPT2(8,7)/ aug-cc-pVTZ	W3X-L // MN15 / Def2TZVP	CASPT2(12,10)[b] // CASPT2(8,7) / aug-cc-pVTZ	CASPT2(12,10) // MN15 / Def2TZVP	Fitted
DMCI	$1 \cdot 9/1$	0.0	0.0	0.0	0.0	*0.0*[b]	*0.0*[b]	
Int1	$1 \cdot 1/3$	-67.62	-68.43	**-64.72**	-65.61	-70.85	-70.25	
Int2	-	-361.5	-361.7	**-357.6**	-358.1	-		
vdw1 (S_0)	-	-	-	-	-	-8.963	-10.44	
vdw1 (S_1)	-	-	-	-	-	-7.540	-9.186	
vdw1 (T_0)	-	-	-	-	-	-8.300	-9.741	
vdw1 (T_1)	-	-	-	-	-	-7.212	-8.852	
vdw2 (S_0)	-	-	-	-6.702	-	-9.800	-10.92	
vdw2 (S_1)	-	-	-	-	-	-7.641	-8.562	
vdw2 (T_0)	-	-	-	-	-	-9.416	-10.16	
vdw2 (T_1)	-	-	-	-	-	-7.441	-8.491	
P[c]	$1 \cdot 6/1$	13.33	12.58	**15.91**	14.77	***15.91***[b]	*14.77*[b]	
ts1	$1 \cdot 3/2$	66.66	66.40	68.61	68.04	69.46	66.26	**65.82**
ts2 (S_0)	$1 \cdot 3/1$	-26.23	-0.9094	**6.806**	-5.813	1.126	-13.00	
ts2 (S_1)	$1 \cdot 3/2$	-	-	-	-	22.79	139.4	
ts2 (T_0)	$1 \cdot 3/2$	-	70.21	-	68.69	7.414	70.04	
ts2 (T_1)	$1 \cdot 3/2$	-	-	-	-	22.20	124.4	
ts3 (S_0)	$1 \cdot 3/2$	-	-	-	-	**-2.820**	-4.987	
ts3 (S_1)	$1 \cdot 3/2$	-	-	-	-	-2.779	-4.487	
ts3 (T_0)	$1 \cdot 3/2$	-	-	-	-	-2.401	-4.537	
ts3 (T_1)	$1 \cdot 3/2$	-	-	-	-	-1.693	-3.851	
ts4 (S_0)	$1 \cdot 3/2$	-	-	-	-	**-8.117**	-10.23	
ts4 (S_1)	$1 \cdot 3/2$	-	-	-	-	4.025	-3.272	
ts4 (T_0)	$1 \cdot 3/2$	-	-	-	-	-6.666	-6.425	
ts4 (T_1)	$1 \cdot 3/2$	-	-	-	-	-4.801	-3.619	

[a] Here σ_{ext} and σ_{int} are the external and internal rotational symmetry numbers, respectively, and m_{opt} is the optical symmetry number.

[b] CASPT2 energies expressed relative to the separated *products* (P), except for ts01 and Int1, which are expressed relative to DMCI. The energy of the reference is set to the W3X-L or W2X value.

[c] Spin-orbit correction 0.8356 kJ mol^{-1} subtracted from computed energy.

Table S4: Zero-kelvin relative enthalpies for stationary points on the DECI (pentan-3-oneoxide) potential-energy surface. The energies are in kJ mol^{-1}. Symmetry numbers for the species are also specified. The fitting errors are 1σ. The **bolded** numbers are the values used in the master-equation simulations.

Species	$\sigma_{\text{ext}} \cdot \sigma_{\text{int}}/m_{\text{opt}}$ [a]	W2X // MN15 / Def2TZVP	W3X-L[b] // CASPT2(8,7)/ aug-cc-pVTZ	CASPT2(12,10)[c,d] // CASPT2(8,7) / aug-cc-pVTZ	CASPT2(12,10) // MN15 / Def2TZVP	Fitted
DECI	$1 \cdot 9/1$	0.0	0.0	*0.0*[d]	*0.0*[d]	
P1[e]	$1 \cdot 9/1$	-13.86	**-10.53**	*-10.53*	*-13.86*	
Int1a	$1 \cdot 9/1$	-69.71	**-65.99**	-71.55	-70.95	
Int1b	$1 \cdot 9/1$	-69.57	**-65.85**	-71.37	-70.77	
vdw1a (S_0)	$1 \cdot 9/1$	-	-	-35.35	-39.02	
vdw1a (S_1)	$1 \cdot 9/1$	-	-	-34.70	-38.54	
vdw1a (T_0)	$1 \cdot 9/1$	-	-	-34.33	-37.96	
vdw1a (T_1)	$1 \cdot 9/1$	-	-	-33.37	-37.21	
vdw1b (S_0)	$1 \cdot 9/1$	-	-	-30.56	-34.23	
vdw1b (S_1)	$1 \cdot 9/1$	-	-	-26.54	-30.37	
vdw1b (T_0)	$1 \cdot 9/1$	-	-	-30.29	-33.92	
vdw1b (T_1)	$1 \cdot 9/1$	-	-	-26.04	-29.88	
vdw2a (S_0)	$1 \cdot 9/1$	-	-	-36.64	-39.95	
vdw2a (S_1)	$1 \cdot 9/1$	-	-	-36.11	-39.22	
vdw2a (T_0)	$1 \cdot 9/1$	-	-	-36.58	-39.52	
vdw2a (T_1)	$1 \cdot 9/1$	-	-	-35.85	-39.09	
vdw2b (S_0)	$1 \cdot 9/1$	-	-	-31.64	-34.95	
vdw2b (S_1)	$1 \cdot 9/1$	-	-	-30.83	-33.94	
vdw2b (T_0)	$1 \cdot 9/1$	-	-	-31.53	-34.46	
vdw2b (T_1)	$1 \cdot 9/1$	-	-	-29.87	-33.12	
ts1a	$1 \cdot 9/2$	78.82	81.03	81.81	78.61	**78.69**
ts1b	$1 \cdot 9/2$	65.49	67.70	68.78	65.58	**65.35**
ts2a (S_0)	$1 \cdot 9/1$	-26.30	**-18.59**	-23.58	-39.90	
ts2a (S_1)	$1 \cdot 9/1$	-	-	26.56	141.0	
ts2a (T_0)	$1 \cdot 9/1$	-	-	-4.038	56.39	
ts2a (T_1)	$1 \cdot 9/1$	-	-	20.19	120.2	
ts2b (S_0)	$1 \cdot 9/1$	-20.14	**-12.43**	-18.24	-34.56	
ts2b (S_1)	$1 \cdot 9/1$	-	-	27.95	142.4	
ts2b (T_0)	$1 \cdot 9/1$	-	-	-2.440	56.99	
ts2b (T_1)	$1 \cdot 9/1$	-	-	26.98	127.0	
ts3a (S_0)	$1 \cdot 9/2$	-	-	**-31.06**	-35.42	
ts3a (S_1)	$1 \cdot 9/2$	-	-	-31.21	-35.11	
ts3a (T_0)	$1 \cdot 9/2$	-	-	-30.64	-34.97	
ts3a (T_1)	$1 \cdot 9/2$	-	-	-30.08	-34.43	
ts3b (S_0)	$1 \cdot 9/2$	-	-	**-25.26**	-29.62	
ts3b (S_1)	$1 \cdot 9/2$	-	-	-25.18	-29.08	
ts3b (T_0)	$1 \cdot 9/2$	-	-	-24.61	-28.94	
ts3b (T_1)	$1 \cdot 9/2$	-	-	-23.98	-28.33	

[a] Here σ_{ext} and σ_{int} are the external and internal rotational symmetry numbers, respectively, and m_{opt} is the optical symmetry number.

[b] **An estimate** based on calculations done on the smaller DMCI system. See equation (6) in the main text and the associated discussion.

[c] **An estimate** based on calculations done on the smaller DMCI system. See equation (7) in the main text and the associated discussion.

[d] CASPT2 energies expressed relative to the separated *products* (P1), except for ts01a/b and Int1a/b, which are expressed relative to DECI. The energy of the reference is set to the W3X-L or W2X value.

[e] Spin-orbit correction 0.8356 kJ mol^{-1} subtracted from computed energy.

Table S5: Zero-kelvin relative enthalpies for stationary points on the DECI (pentan-3-oneoxide) potential-energy surface. The energies are in kJ mol^{-1}. Symmetry numbers for the species are also specified. The fitting errors are 1σ. The **bolded** numbers are the values used in the master-equation simulations.

Species	$\sigma_{ext} \cdot \sigma_{int}/m_{opt}$ [a]	W2X // MN15 / Def2TZVP	W3X-L[b] // CASPT2(8,7)/ aug-cc-pVTZ	CASPT2(14,12)[c,d] // CASPT2(8,7) / aug-cc-pVTZ	CASPT2(14,12) // MN15 / Def2TZVP	Fitted
P2	$1 \cdot 3/1$	-328.5	-	-313.5	-317.9	
(R/S)-Int2	$1 \cdot 9/2$	-379.8	**-375.8**	-367.6	-367.1	
vdw2a (S_0)	$1 \cdot 9/1$	-	-	-36.64	-39.95	
vdw2a (S_1)	$1 \cdot 9/1$	-	-	-35.65	-38.76	
vdw2a (T_0)	$1 \cdot 9/1$	-	-	-36.31	-39.25	
vdw2a (T_1)	$1 \cdot 9/1$	-	-	-35.10	-38.34	
ts4a (S_0)	$1 \cdot 9/2$	-	-	**-29.40**	-33.71	
ts4a (S_1)	$1 \cdot 9/2$	-	-	-22.23	-31.72	
ts4a (T_0)	$1 \cdot 9/2$	-	-	-31.28	-33.23	
ts4a (T_1)	$1 \cdot 9/2$	-	-	-29.83	-30.85	
ts4b (S_0)	$1 \cdot 9/2$	-	-	**-29.25**	-33.56	
ts4b (S_1)	$1 \cdot 9/2$	-	-	-18.97	-28.46	
ts4b (T_0)	$1 \cdot 9/2$	-	-	-28.78	-30.73	
ts4b (T_1)	$1 \cdot 9/2$	-	-	-27.39	-28.40	
(R/S)-ts5	$1 \cdot 3/2$	-	-	-76.10	-75.60	

[a] Here σ_{ext} and σ_{int} are the external and internal rotational symmetry numbers, respectively, and m_{opt} is the optical symmetry number.

[b] **An estimate** based on calculations done on the smaller DMCI system. See equation (6) in the main text and the associated discussion.

[c] **An estimate** based on calculations done on the smaller DMCI system. See equation (7) in the main text and the associated discussion.

[d] CASPT2 energies expressed relative to the separated *products* (P1, see previous table). The energy of the reference is set to the W3X-L or W2X value.

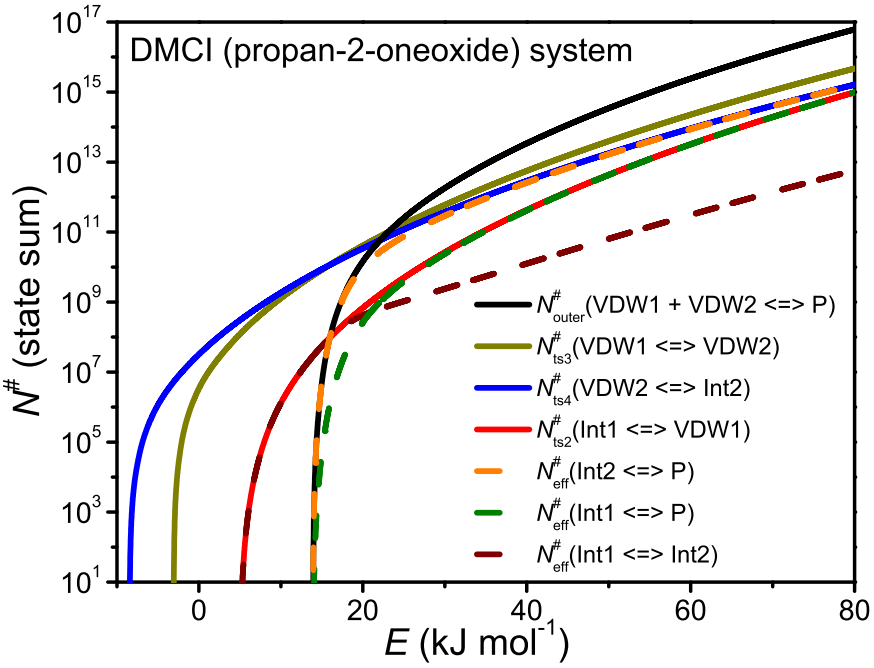

Figure S4: State sums of the transition states in the VDW region of DMCI plotted as a function of energy. Also shown are the effective state sums used in the effective master-equation model.

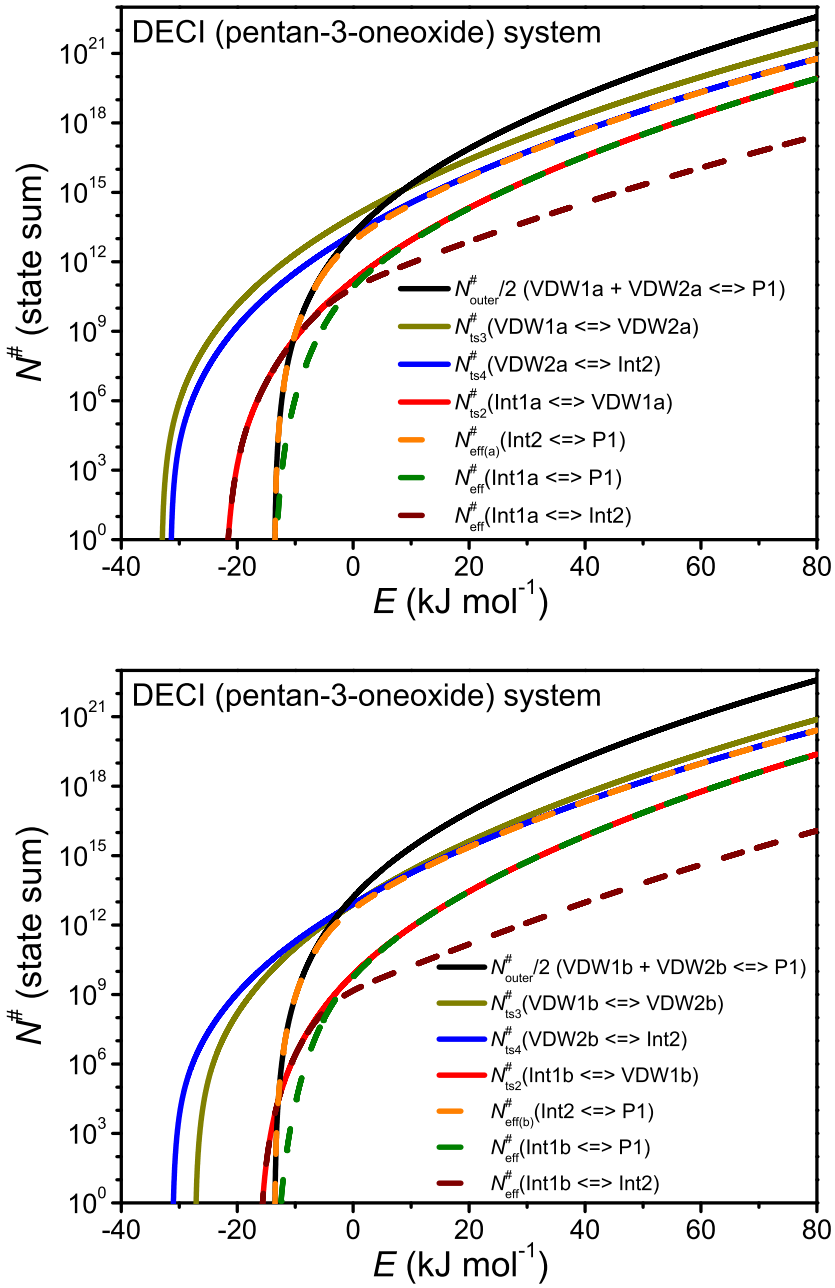

Figure S5: State sums of the transition states in the VDW region of DECI plotted as a function of energy. Also shown are the effective state sums used in the effective master-equation model.

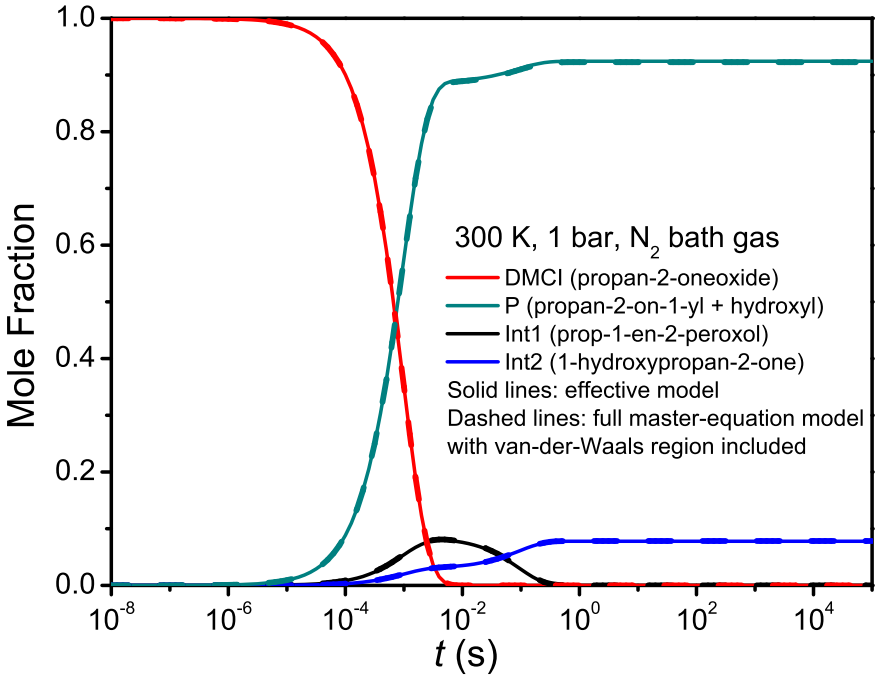

Figure S6: Mole fractions of DMCI, P, Int1, and Int2 plotted as a function if time with the full (dashed lines) and "effective" (solid lines) master-equation models (see main text for details).

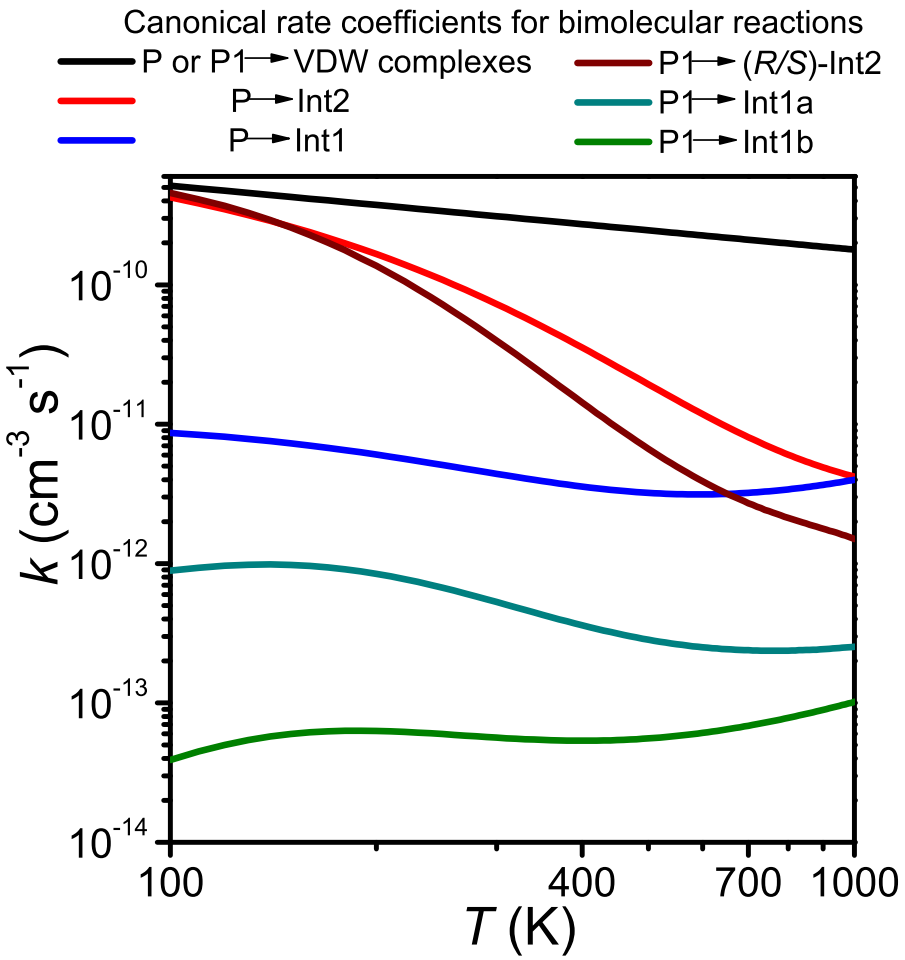

Figure S7: Canonical rate coefficients plotted as a function of temperature for the bimolecular reactions that take place in the DMCI (propan-2-oneoxide) and DECI (pentan-3-oneoxide) systems. Here P, P1, Int1, Int1a, Int1b, Int2, and (R/S)-Int2 stand for propan-2-on-1-yl + hydroxyl, pentan-3-on-2-yl + hydroxyl, prop-1-en-2-peroxol, (Z)-pentan-2-en-3-peroxol, (E)-pentan-2-en-3-peroxol, and (R/S)-2-hydroxypentan-3-one, respectively.

References

[1] J. Peltola, P. Seal, A. Inkilä, A. Eskola, Time-resolved, broadband UV-absorption spectrometry measurements of Criegee intermediate kinetics using a new photolytic precursor: unimolecular decomposition of CH_2OO and its reaction with formic acid, Phys. Chem. Chem. Phys. 22 (2020) 11797–11808. doi:10.1039/D0CP00302F.

[2] J. Peltola, P. Seal, N. Vuorio, P. Heinonen, A. Eskola, Solving the discrepancy between the direct and relative-rate determinations of unimolecular reaction kinetics of dimethyl-substituted Criegee intermediate $(CH_3)_2COO$ using a new photolytic precursor, Phys. Chem. Chem. Phys. 24 (2022) 5211–5219. doi:10.1039/D1CP02270A.

[3] Y.-P. Chang, C.-H. Chang, K. Takahashi, et al., Absolute UV absorption cross sections of dimethyl substituted Criegee intermediate $(CH_3)_2COO$, Chem. Phys. Lett. 653 (2016) 155–160. doi:10.1016/j.cplett.2016.04.082.

[4] F. Liu, J. M. Beames, A. M. Green, M. I. Lester, UV spectroscopic characterization of dimethyl-and ethyl-substituted carbonyl oxides, J. Phys. Chem. A 118 (12) (2014) 2298–2306. doi:10.1021/jp412726z.

[5] L. Franzon, J. Peltola, R. Valiev, N. Vuorio, T. Kurten, A. Eskola, An Experimental and Master Equation Investigation of Kinetics of the CH_2OO + RCN Reactions (R= H, CH_3, C_2H_5) and Their Atmospheric Relevance, J. Phys. Chem. A 127 (2) (2023) 477–488. doi:10.1021/acs.jpca.2c07073.

[6] E. Westley, M. J. Sowden, N. L. Magann, K. L. Horvath, K. P. Connor, M. S. Sherburn, Substituted tetraethynylethylene–tetravinylethylene hybrids, J. Am. Chem. Soc. 144 (2) (2022) 977–986. doi:10.1021/jacs.1c11598.

[7] R. Y. Tien, P. I. Abell, Kinetics and stereochemistry of the gas-phase addition of HBr to methyl-substituted allenes, J. Org. Chem. 35 (4) (1970) 956–960. doi:10.1021/jo00829a019.

[8] M. C. Smith, W. Chao, K. Takahashi, K. A. Boering, J. J.-M. Lin, Unimolecular Decomposition Rate of the Criegee Intermediate $(CH_3)_2COO$ Measured Directly with UV Absorption Spectroscopy, J. Phys. Chem. A 120 (27) (2016) 4789–4798. doi:10.1021/acs.jpca.5b12124.

[9] J. Peltola, P. Heinonen, A. Eskola, Direct Kinetic Measurements of a Cyclic Criegee Intermediate; Unimolecular Decomposition of *c*-$(CH_2)_5COO$, J. Phys. Chem. Lett. 15 (2024) 5331–5336. doi:10.1021/acs.jpclett.4c00554.